

# Ultrasound Specific Similarity Measures for Three-Dimensional Mosaicing

Christian Wachinger and Nassir Navab

Computer Aided Medical Procedures (CAMP), Technische Universität München,  
Boltzmannstr. 3, 85748 Garching, Germany.

## ABSTRACT

The introduction of 2D array ultrasound transducers enables the instantaneous acquisition of ultrasound volumes in the clinical practice. The next step coming along is the combination of several scans to create compounded volumes that provide an extended field-of-view, so called mosaics. The correct alignment of multiple images, which is a complex task, forms the basis of mosaicing. Especially the simultaneous intensity-based registration has many properties making it a good choice for ultrasound mosaicing in comparison to the pairwise one.

Fundamental for each registration approach is a suitable similarity measure. So far, only standard measures like SSD, NNC, CR, and MI were used for mosaicing, which implicitly assume an additive Gaussian distributed noise. For ultrasound images, which are degraded by speckle patterns, alternative noise models based on multiplicative Rayleigh distributed noise were proposed in the field of motion estimation.

Setting these models into the maximum likelihood estimation framework, which enables the mathematical modeling of the registration process, led us to ultrasound specific bivariate similarity measures. Subsequently, we used an extension of the maximum likelihood estimation framework, which we developed in a previous work, to also derive multivariate measures. They allow us to perform ultrasound specific simultaneous registration for mosaicing. These measures have a higher potential than afore mentioned standard measures since they are specifically designed to cope with problems arising from the inherent contamination of ultrasound images by speckle patterns. The results of the experiments that we conducted on a typical mosaicing scenario with only partly overlapping images confirm this assumption.

**Keywords:** Registration

## 1. DESCRIPTION OF PURPOSE

The recent introduction of 2D array ultrasound (US) transducers on the market will soon lead to a paradigm shift in sonography, moving from 2D to 3D image acquisition. This shift may be further accelerated by the next generation of ultrasound transducers with the CMUT (Capacitive Micromachined Ultrasound Transducer) technology, which are currently in the phase of prototyping, offering superior and efficient volumetric imaging at a lower cost. One of the major drawbacks that remains though, is the limited field-of-view (FOV) of the acquired images. The idea of mosaicing is to address this issue by stitching several images taken from different poses to create a larger one. An example mosaic consisting of 4 acquisitions of a baby phantom is shown in figure 1.

### 1.1 Clinical Value

The usage of ultrasound mosaicing provides the sonographers not just with a compounded volume of higher quality; recent studies also state a couple of other clinical advantages that come along with the extended FOV. First, the spatial relationship among structures that are too large for a single volume is easier to understand.<sup>1</sup> Second, sonographers have the flexibility to visualize anatomical structures from a variety of different angles.<sup>2,3</sup> Third, size and distance measurements of large organs are possible.<sup>1,4</sup> Fourth, individual structures within a broader context can be identified by having an image of the whole examination area.<sup>5</sup> And last, because of the increased features in the compounded view, specialists that are used to other modalities than ultrasound can better understand the spatial relationships of anatomical structures;<sup>6</sup> helping to bridge the gap between the modalities and making it easier to convey sonographic findings to other experts.

---

Further author information: (Send correspondence to C.W.)

C.W.: E-mail: wachinge@cs.tum.edu

N.N.: E-mail: navab@cs.tum.edu

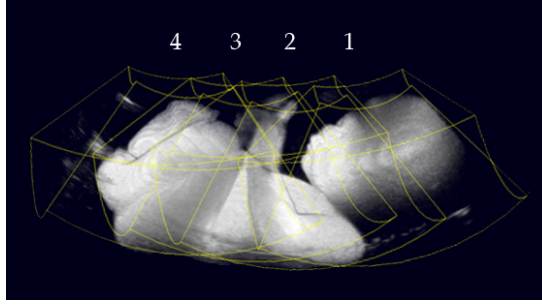


Figure 1. Baby Phantom

But it is not just the improvement of already existing clinical workflows, the creation of high quality mosaics may also create new medical applications for ultrasound that do not yet exist at all or are reserved for other modalities, so far. Finally, three-dimensional mosaicing could be the application helping 3D imaging to gain widespread access in the clinical practice, which it has not yet,<sup>7</sup> although there are studies giving evidence that 3D imaging is superior to 2D imaging.<sup>8</sup>

## 1.2 Mosaicing Strategies

Crucial for a high quality stitching is the correct calculation of the spatial relationship of the acquisitions to each other. In our earlier work,<sup>9</sup> we investigated different rigid intensity-based registration strategies, which could be used in the mosaicing scenario. The major problems that we have identified are the significant overlap dependency of bivariate similarity measures, favoring a total overlap of the volumes, and the error accumulation by using a sequence of pairwise registrations. Simultaneous registration, instead, solved these problems; taking all the images into consideration reduces the overlap dependency and accumulation errors do not show up since they are dealt with intrinsically during the registration process. Moreover, in contrast to the bivariate ones, multivariate similarity measures take the whole available information into account being especially important for viewing angle dependent US images.

## 1.3 Problem Statement

Sonography suffers from artifacts caused by coherent wave interference known as speckle. Speckle limits low resolution image contrast and may even obscure true structures in high contrast regions. Therefore most of the works are interested in reducing the speckle noise in the images by low-pass filtering, *e.g.* with a Gaussian filter.<sup>10,11</sup> Nevertheless, a recent work on freehand 3D ultrasound uses speckle for the registration of the slices.<sup>12</sup> This requires a permanent stream of high-resolution scans from a similar viewing angle with a small spacing between slices. Hence, the same speckle patterns will be visible on successive 2D images.

So far, only the standard similarity measures SSD, NCC, CR, and MI were used for 3D mosaicing, which are not specifically designed for US images. Modeling the registration process mathematically by a maximum-likelihood estimation (MLE) allows to derive these four measures by assuming a Gaussian distributed noise. But due to the influence of speckle patterns in US images, it was shown that Rayleigh distributed noise is more appropriate.<sup>13</sup> Based on this noise assumption Strintzis, Kokkindis<sup>14</sup> and Cohen, Dinstein<sup>15</sup> developed likelihood terms for US motion estimation denoted by  $SK_1$ ,  $SK_2$  and  $CD_1$ ,  $CD_2$ , respectively.

We will use these ultrasound specific likelihood terms to deduce bivariate similarity measures and, in a second step, extend them to multivariate measures to make them work in our simultaneous registration framework, used for 3D ultrasound mosaicing. The good results of Boukerroui et al.<sup>16</sup> and Revell et al.,<sup>17</sup> who used a bivariate extension of  $CD_2$ , further encouraged our intentions.

## 2. METHOD

In this section we will first present the deduction of ultrasound specific bivariate similarity measures and then, in a second step, extend them to multivariate ones. Throughout the report,  $u$  and  $v$  are the images,  $T$  the rigid transformation,  $f$  the

intensity mapping, and  $\varepsilon$  the random variable a certain noise distribution. The log-likelihood function that we maximize in the MLE framework is given by

$$\log \mathcal{L}(T, \varepsilon, f) = \log P(u|v, T, \varepsilon, f) \quad (1)$$

$$= \log \prod_{x_k \in \Omega} P(u_k|v_k, T, \varepsilon, f). \quad (2)$$

with the i.i.d. assumption on the spatial domain  $\Omega$ . When deriving standard similarity measures like SSD, CR, NCC, and MI, one assumes a Gaussian distributed additive noise, leading to the imaging model

$$u(x) = f(v(T(x))) + \varepsilon. \quad (3)$$

Since we are interested in mono-modal registration, we set the mapping to the identity  $f = \text{id}$ . The log-likelihood function is

$$\log \mathcal{L}(T, \varepsilon) = -N \cdot \log \sqrt{2\pi\sigma} - \frac{1}{2} \sum_{x_k \in \Omega_u} \frac{(u(x_k) - f(v(T(x_k))))^2}{\sigma^2} \quad (4)$$

with the variance  $\sigma^2$ , the overlapping region between the two images  $\Omega_u$ , and the cardinality of the overlap  $N = |\Omega_u|$ . Based on this equation, one can look in the articles of Roche et al.<sup>18</sup> and Viola<sup>19</sup> to find the derivations of the afore mentioned measures.

### SK<sub>1</sub>: Multiplicative Rayleigh noise

The first model proposed by Strintzis, Kokkinidis<sup>14</sup> is to use multiplicative Rayleigh distributed noise to represent speckle patterns. The imaging process is described by

$$u(x) = v(T(x)) \cdot \varepsilon \quad (5)$$

with the Rayleigh distribution

$$P(y) = \frac{\pi \cdot y}{2} \cdot \exp\left(-\frac{\pi \cdot y^2}{4}\right), y > 0 \quad (6)$$

having the variance  $\frac{2}{\pi}$ . Setting it into the MLE framework, equation (2), leads to:

$$\log \mathcal{L}(T, \varepsilon) = \log \prod_{x_k \in \Omega} \frac{1}{v(T(x_k))} P\left(\frac{u(x_k)}{v(T(x_k))}\right) \quad (7)$$

$$\approx \sum_{x_k \in \Omega} \log\left(\frac{u(x_k)}{v(T(x_k))^2}\right) - \frac{\pi}{4} \frac{u(x_k)^2}{v(T(x_k))^2}. \quad (8)$$

### SK<sub>2</sub>: Signal dependent Gaussian noise

The second model proposed by Strintzis and Kokkinidis<sup>14</sup> uses signal dependent additive Gaussian distributed noise, being expressed by

$$u(x) = v(T(x)) + \sqrt{v(T(x))} \cdot \varepsilon \quad (9)$$

with the Gaussian distribution

$$P(y) = \frac{1}{\sqrt{2\pi\sigma}} \exp\left(-\frac{y^2}{2 \cdot \sigma^2}\right), y > 0 \quad (10)$$

and  $\sigma^2$  the variance. Setting it once again into the MLE framework leads to:

$$\log \mathcal{L}(T, \varepsilon) = \log \prod_{x_k \in \Omega} \frac{1}{\sqrt{v(T(x_k))}} \exp\left(-\frac{[u(x_k) - v(T(x_k))]^2}{2 \cdot \sigma^2 \cdot v(T(x_k))}\right) \quad (11)$$

$$= \sum_{x_k \in \Omega} -\log[v(T(x_k))] - \frac{[u(x_k) - v(T(x_k))]^2}{2 \cdot \sigma^2 \cdot v(T(x_k))}. \quad (12)$$

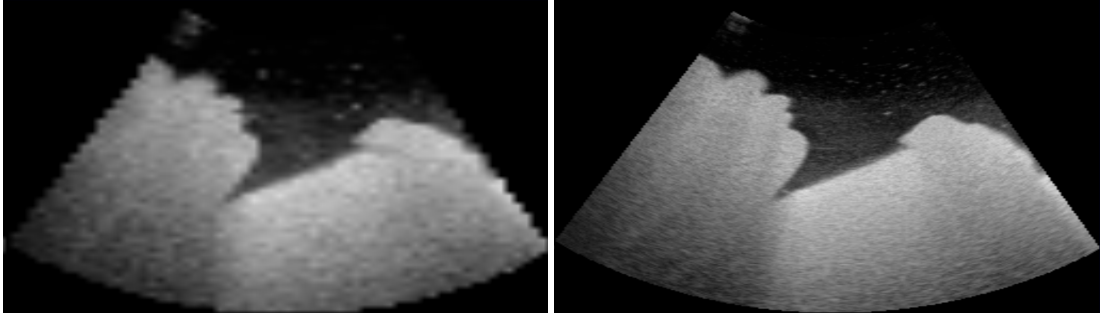


Figure 2. Speckle noise in baby phantom on low and high resolution.

### CD<sub>1</sub>: Division of Rayleigh noises

The noise models of Strintzis, Kokkindis<sup>14</sup> consider only one image to be degraded by noise, the other one has to be noiseless, which is not possible in practice. Cohen, Dinstein<sup>15</sup> assume each image to be contaminated by multiplicative Rayleigh noises  $\varepsilon_1$  and  $\varepsilon_2$ , respectively. This leads to the following noise model

$$u(x) = v(T(x)) \cdot \varepsilon \quad (13)$$

with

$$\varepsilon = \frac{\varepsilon_1}{\varepsilon_2} \quad (14)$$

and the probability density function

$$P(y) = \frac{2 \cdot y}{(y^2 + 1)^2}, y > 0. \quad (15)$$

The probability density function results from the division of two Rayleigh distributed random variables.<sup>20</sup> The log-likelihood function is:

$$\log \mathcal{L}(T, \varepsilon) = \log \prod_{x_k \in \Omega} \frac{1}{v(T(x_k))} P\left(\frac{u(x_k)}{v(T(x_k))}\right) \quad (16)$$

$$= \log \prod_{x_k \in \Omega} \frac{1}{v(T(x_k))} \frac{2 \cdot \frac{u(x_k)}{v(T(x_k))}}{\left(\left(\frac{u(x_k)}{v(T(x_k))}\right)^2 + 1\right)^2} \quad (17)$$

$$= \sum_{x_k \in \Omega} \log \frac{2 \cdot u(x_k)}{v(T(x_k))^2} - 2 \cdot \log \left[ \left(\frac{u(x_k)}{v(T(x_k))}\right)^2 + 1 \right] \quad (18)$$

$$\approx \sum_{x_k \in \Omega} \log u(x_k) - \log v(T(x_k)) - \log \left[ \left(\frac{u(x_k)}{v(T(x_k))}\right)^2 + 1 \right]. \quad (19)$$

### CD<sub>2</sub>: Logarithm of division of Rayleigh noises

The second model by Cohen, Dinstein<sup>15</sup> considers next to the noise contamination of both images also the log-compressed nature of ultrasound images by applying the logarithm to equation (13), leading to:

$$\log u(x) = \log(v(T(x)) \cdot \varepsilon) \quad (20)$$

$$= \log v(T(x)) + \log \varepsilon. \quad (21)$$

With setting  $\tilde{u}(x) = \log u(x)$  and  $\tilde{v}(x) = \log v(T(x))$

$$\varepsilon(x) = \exp(\tilde{u}(x) + \tilde{v}(x)) \quad (22)$$

SK <sub>1</sub>	SK <sub>2</sub>	CD <sub>1</sub>	CD <sub>2</sub>
$\sum_{i \neq j} \mathbb{E}_k \left[ \log \left( \frac{i_k}{j_k} \right) - \frac{\pi}{4} \frac{i_k^2}{j_k^2} \right]$	$\sum_{i \neq j} \mathbb{E}_k \left[ \log j_k + \frac{(i_k - j_k)^2}{j_k} \right]$	$\sum_{i \neq j} \mathbb{E}_k \left[ \log \frac{i_k}{j_k} \left( \left( \frac{i_k}{j_k} \right)^2 + 1 \right)^{-2} \right]$	$\sum_{i \neq j} \mathbb{E}_k \left[ \tilde{i}_k - \tilde{j}_k - \log(e^{2(\tilde{i}_k - \tilde{j}_k)} + 1) \right]$

Table 1. Multivariate ultrasound specific similarity measures.

leading to the log-likelihood function:

$$\log \mathcal{L}(T, \varepsilon) = \log \prod_{x_k \in \Omega} \frac{\exp(\tilde{u}(x_k))}{\exp(\tilde{v}(x_k))} \cdot P(\exp(\tilde{u}(x_k) - \tilde{u}(x_k))) \quad (23)$$

$$= \log \prod_{x_k \in \Omega} \frac{\exp(\tilde{u}(x_k))}{\exp(\tilde{v}(x_k))} \cdot \frac{2 \cdot \exp(\tilde{u}(x_k) - \tilde{u}(x_k))}{[\exp(\tilde{u}(x_k) - \tilde{u}(x_k))^2 + 1]^2} \quad (24)$$

$$= \log \prod_{x_k \in \Omega} \frac{2 \cdot \exp(2(\tilde{u}(x_k) - \tilde{u}(x_k)))}{[\exp(2(\tilde{u}(x_k) - \tilde{u}(x_k))) + 1]^2} \quad (25)$$

$$\approx \sum_{x_k \in \Omega} \tilde{u}(x_k) - \tilde{v}(x_k) - \log[\exp(2(\tilde{u}(x_k) - \tilde{v}(x_k))) + 1]. \quad (26)$$

## 2.1 Multivariate Similarity Measures

Essential for the usage of simultaneous registration strategies are multivariate similarity measures. In our previous work,<sup>9</sup> we deduced a novel way of creating multivariate similarity measures by summing up their bivariate counterparts. In terms of the MLE framework, with setting  $u_i^\dagger = u_i(T_i(\cdot))$ , the log-likelihood function is

$$\log \mathcal{L}(\mathcal{T}, \vec{\varepsilon}) = \sum_i \log P(u_i^\dagger | u_1^\dagger, \dots, u_{i-1}^\dagger, u_{i+1}^\dagger, \dots, u_n^\dagger, \vec{\varepsilon}) \quad (27)$$

$$= \sum_{i \neq j} \log P(u_i^\dagger | u_j^\dagger, \varepsilon_{i,j}) \quad (28)$$

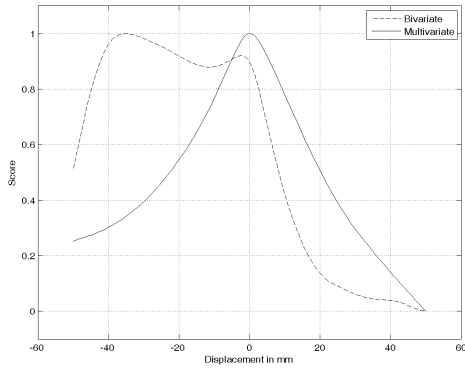
with the noise vector  $\vec{\varepsilon} = (\varepsilon_{i,j})_{i,j \in \{1, \dots, n\}, (i \neq j)}$ , the  $n$  images  $\mathcal{U} = \{u_1, \dots, u_n\}$ , and the corresponding transformations  $\mathcal{T} = \{T_1, \dots, T_n\}$ . Each summand corresponds to the bivariate formula of equation (2) from which we started the derivation of the bivariate measures. A summary of the multivariate extensions of the similarity measures is shown in table 1. To make the table clearer we set  $i_k = u_i(T_i(x_k))$ ,  $j_k = u_j(T_j(x_k))$ ,  $\tilde{i}_k = \log u_i(T_i(x_k))$ , and  $\tilde{j}_k = \log u_j(T_j(x_k))$ .

## 3. RESULTS

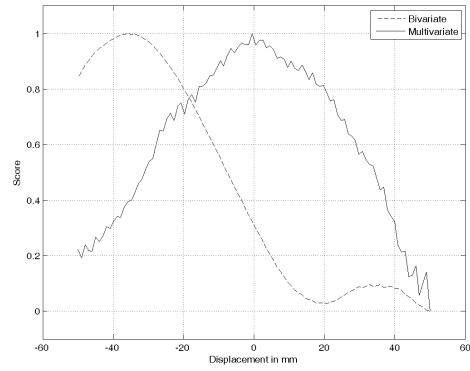
An evaluation of the presented bi- and multivariate similarity measures was done on high and low resolution 3D ultrasound acquisitions of a baby phantom. The high resolution data set has a resolution of  $256^3$  voxel and the low resolution data set  $64^3$  voxel. The reason for using two different resolutions is to find out whether ultrasound-specific similarity measures make only sense, when imaging speckle at a high resolution. The data sets consists of four sequential acquisitions, see figure 1. We plot the similarity measures by moving the second volume along the cranio-caudal axis and evaluate the associated score values. The correct alignment of the volumes is at a displacement of 0.0 mm, and the total overlap of the volumes is at -37.0 mm displacement. As a reference we also show the plot of SSD, see figure 3(a) and 4(a), respectively.

Like we mentioned already in our previous work,<sup>9</sup> the bivariate similarity measures are significantly overlap dependent. The bivariate plot of SSD for example, only has a local maximum at the correct position whereas the global maximum is at the position of total overlap. Also SK<sub>1</sub>, SK<sub>2</sub>, and CD<sub>1</sub> favor the total overlap, see figure 3(b) - 3(d) and 4(b) - 4(d), respectively. The best performance shows CD<sub>2</sub>, although there is still a local maximum at the total overlap, the global maximum is at the correct position, see figure 3(e) and 4(e). For the bivariate measures, we observe that there is no difference between working on high or low resolution data.

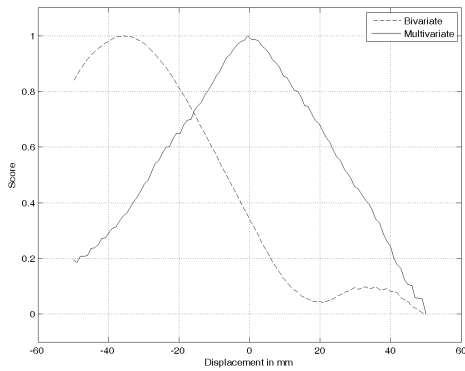
In the multivariate case, in contrast, the measures show a clear maximum at the correct position and the similarity curve becomes smoother when working on high resolution data sets. The graph of SK<sub>1</sub>, for example, is not very smooth in the



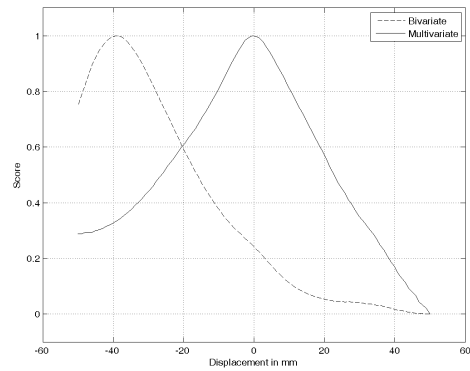
(a) SSD



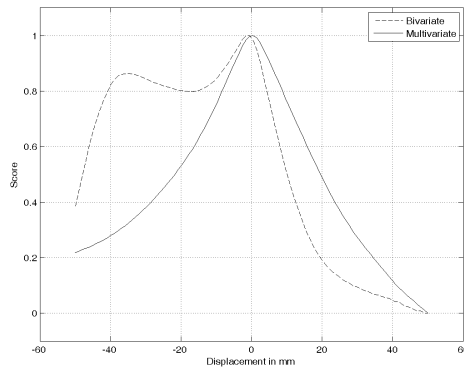
(b) SK<sub>1</sub>



(c) SK<sub>2</sub>



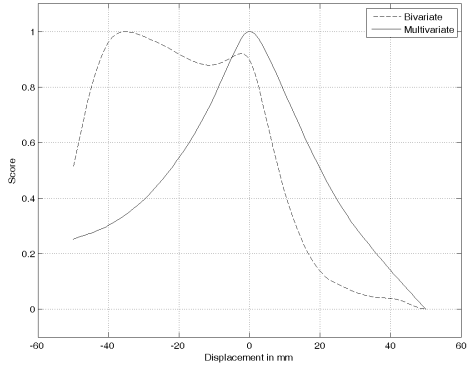
(d) CD<sub>1</sub>



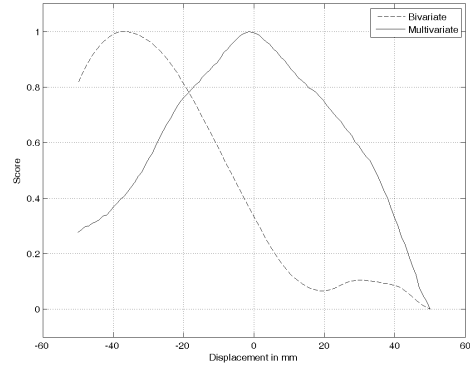
(e) CD<sub>2</sub>

Figure 3. Similarity plots of the measures in table 1 together with SSD on low resolution baby phantom. The bivariate measures are shown by a dashed line, the multivariate ones by a solid line (x-axis: displacement in mm, y-axis: score).

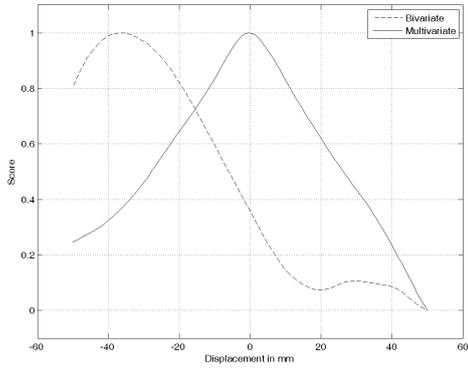
low resolution case and may therefore pose problems to the optimizer. The shape of the cost function obtained with SK<sub>2</sub> is smoother, but the best results were received with CD<sub>1</sub> and CD<sub>2</sub>. These results are corresponding to them of Cohen, Dinstein<sup>15</sup> and Boukerroui et al.<sup>16</sup>



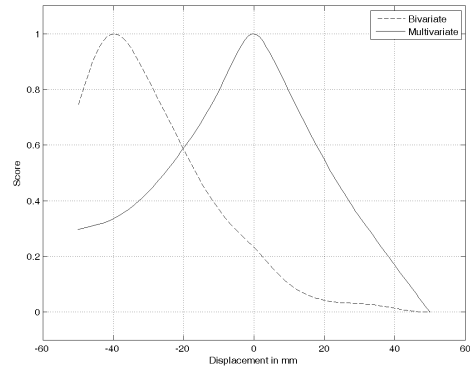
(a) SSD



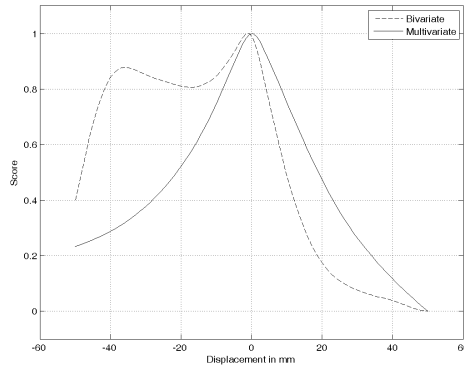
(b) SK<sub>1</sub>



(c) SK<sub>2</sub>



(d) CD<sub>1</sub>



(e) CD<sub>2</sub>

Figure 4. Similarity plots of the measures in table 1 together with SSD on high resolution baby phantom. The bivariate measures are shown by a dashed line, the multivariate ones by a solid line (x-axis: displacement in mm, y-axis: score).

#### 4. NEW OR BREAKTHROUGH WORK TO BE PRESENTED

Three-dimensional ultrasound mosaicing has so far only been done with standard similarity measures where the characteristics of US images have not been taken into consideration. In this article, we deduced bivariate ultrasound specific similarity measures for SK<sub>1</sub>, SK<sub>2</sub>, and CD<sub>1</sub>. The deduction of CD<sub>2</sub> has already been presented earlier by Boukerroui et al.<sup>16</sup> Moreover, we presented multivariate extensions for these measures, making simultaneous registration with ultrasound

specific measures possible.

## 5. CONCLUSION

We have used the maximum likelihood block matching motion estimation methods of Strintzis, Kokkinidis and Cohen, Dinstein to derive ultrasound specific similarity measures. For this purpose, we set the proposed noise models into the maximum likelihood estimation framework to derive bivariate measures and subsequently extended them to multivariate similarity measures by using our earlier developed approach.<sup>9</sup> We evaluated the performance of the proposed similarity measures for three-dimensional ultrasound mosaicing. The bivariate similarity measures had problems with the varying amount of overlap, clearly favoring a total overlap of the volumes. Only CD<sub>2</sub> performed well and found the correct spatial relationship of the volumes. This can be attributed to the consideration of the log-compression of the US images.

In the case of multivariate similarity measures the general performance was much better, but also here the ones of Cohen, Dinstein performed better than the ones of Strintzis, Kokkinidis. The reasons may be found in the better adapted noise model, which considers both images to be degraded by a Rayleigh distributed noise. Further test will have to be conducted to better differentiate the multivariate similarity measures, but the results from the bivariate ones already indicated the necessity for ultrasound specific measures.

**Acknowledgment** We thank Siemens Corporate Research (Princeton, USA) for generously providing the images.

## REFERENCES

1. S. H. Kim, B. I. Choi, K. W. Kim, K. H. Lee, and J. K. Han, "Extended Field-of-View Sonography: Advantages in Abdominal Applications," *Journal of Ultrasound in Medicine* **22**(4), pp. 385–394, 2003.
2. P. Peetrons, "Ultrasound of muscles," *European Radiology* **12**(1), pp. 35–43, 2002.
3. Y. Leung, A. Roshier, S. Johnson, R. Kerslake, and D. McNally, "Demonstration of the appearance of the paraspinal musculoligamentous structures of the cervical spine using ultrasound.," *Clin Anat* **18**(2), pp. 96–103, 2005.
4. M. Ying and M.-H. Sin, "Comparison of extended field of view and dual image ultrasound techniques: Accuracy and reliability of distance measurements in phantom study," *Ultrasound in Medicine & Biology* **31**, pp. 79–83, Jan 2005.
5. C. Dietrich, A. Ignee, M. Gebel, B. Braden, and G. Schuessler, "Imaging of the abdomen," *Z Gastroenterol* **40**, pp. 965–970, 2002.
6. W. Henrich, A. Schmider, S. Kjos, B. Tutschek, and J. W. Dudenhausen, "Advantages of and applications for extended field-of-view ultrasound in obstetrics," *Archives of Gynecology and Obstetrics* **V268**, pp. 121–127, Jun 2003.
7. H. Kuhl, M. Schreckenberger, D. Rulands, M. Katoh, W. Schafer, G. Schummers, A. Bucker, P. Hanrath, and A. Franke, "High-resolution transthoracic real-time three-dimensional echocardiography Quantitation of cardiac volumes and function using semi-automatic border detection and comparison with cardiac magnetic resonance imaging," *Journal of the American College of Cardiology* **43**(11), pp. 2083–2090, 2004.
8. C. Jenkins, K. Bricknell, L. Hanekom, and T. Marwick, "Reproducibility and accuracy of echocardiographic measurements of left ventricular parameters using real-time three-dimensional echocardiography," *Journal of the American College of Cardiology* **44**(4), pp. 878–886, 2004.
9. C. Wachinger, W. Wein, and N. Navab, "Three-dimensional ultrasound mosaicing," in *International Conference on Medical Image Computing and Computer-Assisted Intervention (MICCAI)*, (Brisbane, Australia), October 2007.
10. A. H. Gee, G. M. Treece, R. W. Prager, C. J. C. Cash, and L. H. Berman, "Rapid registration for wide field-of-view freehand 3d ultrasound.," *IEEE Trans. Med. Imaging* **22**(11), pp. 1344–1357, 2003.
11. G. P. Penney, J. M. Blackall, M. S. Hamady, T. Sabharwal, A. Adam, and D. J. Hawkes, "Registration of freehand 3d ultrasound and magnetic resonance liver images," *Medical Image Analysis* **8**, pp. 81–91, March 2004.
12. R. J. Housden, A. H. Gee, G. M. Treece, and R. W. Prager, "Subsample interpolation strategies for sensorless freehand 3d ultrasound.," *Ultrasound Med Biol* **32**, pp. 1897–904, 2006.
13. C. Kotropoulos, X. Magnisalis, I. Pitas, and M. Strintzis, "Nonlinear ultrasonic image processing based on signal-adaptive filters and self-organizing neural networks," *Image Processing, IEEE Transactions on* **3**(1), pp. 65–77, 1994.
14. M. Strintzis and I. Kokkinidis, "Maximum likelihood motion estimation in ultrasound image sequences," *Signal Processing Letters, IEEE* **4**(6), pp. 156–157, 1997.
15. B. Cohen and I. Dinstein, "New maximum likelihood motion estimation schemes for noisy ultrasound images," *Pattern Recognition* **35**(2), pp. 455–463, 2002.
16. D. Boukerroui, J. Noble, and M. Brady, "Velocity estimation in ultrasound images: a block matching approach.," *Inf Process Med Imaging* **18**, pp. 586–98, 2003.
17. J. Revell, M. Mirmehdi, and D. McNally, "Combined ultrasound speckle pattern similarity measures," in *Medical Image Understanding and Analysis*, pp. 149–153, BMVA Press, September 2004.

18. A. Roche, G. Malandain, and N. Ayache, "Unifying maximum likelihood approaches in medical image registration," *International Journal of Imaging Systems and Technology: Special Issue on 3D Imaging* **11**(1), pp. 71–80, 2000.
19. P. A. Viola, *Alignment by Maximization of Mutual Information*. Ph.d. thesis, Massachusetts Institute of Technology, 1995.
20. A. Papoulis and U. S. Pillai, *Probability, Random Variables and Stochastic Processes*, McGraw-Hill, December 2001.